Korean J. Chem. Eng., 33(10), 2849-2857 (2016)
DOI: 10.1007/s11814-016-0148-9

pISSN: 0256-1115
eISSN: 1975-7220

Sulfidation and regeneration of iron-based sorbents supported on activated-chars prepared by pressurized impregnation for coke oven gas desulfurization

Jinxiao Dou*, Yongqi Zhao*, Arash Tahmasebi*, and Jianglong Yu*,,†**

*Key Laboratory for Advanced Coal and Coking Technology of Liaoning Province, School of Chemical Engineering, University of Science and Technology Liaoning, Anshan 114051, China
**Chemical Engineering, University of Newcastle, Callaghan, NSW 2308, Australia
(*Received 11 April 2016 • accepted 31 May 2016*)

Abstract−The sulfidation and regeneration properties of lignite char-supported iron-based sorbent for coke oven gas (COG) desulfurization prepared by mechanical stirring (MS), ultrasonic assisted impregnation (UAI), and high pressure impregnation (HPI) were investigated in a fixed-bed reactor. During desulfurization, the effects of process parameters on sulfidation properties were studied systematically. The physical and chemical properties of the sorbents were analyzed by X-ray diffraction (XRD), scanning electron microscope coupled with energy dispersive spectroscopy (SEM-EDS), Fourier transform infrared (FTIR) and BET surface area analysis. The results of desulfurization experiments showed that high pressure impregnation (HPI) enhanced the sulfidation properties of the sorbents at the breakthrough time for char-supported iron sorbents. HPI method also increased the surface area and pore volume of sorbents. Sulfur capacity of sorbents was enhanced with increasing sulfidation temperatures and reached its maximum value at 400 °C. It was observed that the presence of steam in coke oven gas can inhibit the desulfurization performance of sorbent. SO_2 regeneration of sorbent resulted in formation of elemental sulfur. HPIF10 sorbent showed good stability during sulfide-regeneration cycles without changing its performance significantly.

Keywords: Lignite Char, Coke Oven Gas, Pressurized Impregnation, Iron-based Sorbent, Regeneration

INTRODUCTION

Coke oven gas (COG), a by-product of the coking industry, has significant industrial value for heat generation, hydrogen production, carbinol production, and direct reduction of iron. COG is considered a valuable and clean form of energy [1]. However, COG produced from the coking industry contains significant quantities of undesirable impurities, such as hydrogen sulfide (H_2S), ammonia (NH_3) and hydrogen cyanide (HCN) [2,3]. The corrosive nature of sulfur may cause corrosion of the equipment and poison the catalyst. Therefore, COG desulfurization is important for environmental protection and prevention of corrosion of process components such as catalysts, fuel cells, internal combustion engines and turbines [4,5]. In general, coke oven gas desulfurization can be divided into wet desulfurization technologies and dry desulfurization processes. Wet coal gas desulfurization can be used for the efficient removal of H_2S, but this method requires large equipment and complex systems with associated high investment and operating costs [6]. However, dry desulfurization processes have the potential to significantly improve the thermal efficiency and reduce the capital and operating costs. The costly fuel cooling and heating process and waste water treatment can be avoided in dry desulfurization processes. Furthermore, dry desulfurization has the potential to simultaneously remove sulfur and nitrogen containing impurities, as well as Hg [7,8].

The use of lignite char supported sorbents for dry desulfurization processes has been reported by the authors and other researchers [9-12]. Preparation of novel sorbents with high desulfurization performance is essential to achieve a higher sulfur removal and to improve the efficiency of coal utilization processes. Properties and structure of sorbents depend upon their preparation methods [9, 13,14]. Generally, for the sake of high reactivity of sorbent, it is desired to deposit the active components on the exterior and internal surfaces (pore structure) of the support materials in order to have a better dispersion. The high pressure impregnation (HPI) method has recently gained much attention as a promising impregnation method. The HPI method has diverse applications in chemical processes and environmental science [15,16]. High dispersion of active components on pore structure of the carrier can be achieved by using this technique. The HPI method can increase the specific surface area and the porosity of activated semi-coke, which then improves the desulfurization performance of the sorbent [16]. As mentioned, the use of HPI in sorbent preparation is a promising method due to the higher content of metal loaded on the lignite char. In addition, this process does not require any additional acid or alkali solution during the preparation process, thus reducing the environmental pollution. In our previous study, ammonia was used as the agent for the preparation of sorbents. However, the combustion of ammonia was a concern [12,17]. It is crucial to choose the appropriate sorbent for removing H_2S and COS from coke oven gas. Various desulfurization sorbents such as iron-based oxides, zinc-based oxides, copper-based oxides, and mixed

†To whom correspondence should be addressed.
E-mail: jianglongyu@163.com

metal oxides have been widely investigated for coal gas desulfurization [18-20]. Iron oxide sorbents, due to their high sulfur capacity, low cost, and simple operation, have also been widely used for removing H_2S, SO_2 and NO_X, from coal-based gases [21]. The reactivity of char supported nano-sized iron sorbent can further be improved by doping with transition metals. It was reported that the addition of Mo, Cu, Mn, and Zn oxides to Fe_3O_4 results in an increase of the breakthrough capacity during coal gas desulfurization [23]. Apart from a good desulfurization behavior, the spent sorbent after sulfidation needs to be regenerated and show a good stability in multiple desulfurization-regeneration cycles to satisfy the industrial requirements. Compared to O_2 and H_2O regeneration, SO_2 regeneration of the spent sorbent has the advantage of elemental sulfur formation, and the sorbent sintering can be avoided [24].

In the present study, lignite char supported iron-based sorbents were prepared by MS, UAI and HPI methods. The objective was to evaluate the desulfurization performance of such sorbents in simulated COG. The effects of operating parameters such as temperature, steam content, and regeneration on the sulfidation properties of sorbents were systematically investigated. Also, to understand the structural changes, the sorbents were characterized by XRD, FTIR, BET and SEM-EDS before and after desulfurization.

EXPERIMENTAL SECTION

1. Preparation of Sorbent

Hailar lignite from the Inner Mongolia region of China was used in this study. The sample was crushed and sieved to 75-125 μm particle size and then dried under nitrogen at 105 °C. The dried coal samples were acid-washed using HCl aqueous solution (4 mol/L) for 12 hours. The slurry was then filtered and washed using deionized water until the pH value of the filtrate reached 5.0-5.5. The acid-washed coal was mixed with a solution of ferric nitrate (Sinopharm Chemical Reagent Co. Ltd.) with a mass ratio of coal to ferric nitrate of 10 : 1. The samples were impregnated about 2 hours using MS, HPI and UAI methods at 100 °C. The samples were dried at 105 °C under nitrogen, and gasified for 30 minutes with steam (15% vol balanced with nitrogen) in a fluidized-bed quartz reactor at 700 °C. These sorbents were assigned as MSF10, UAIF10 and HPIF10. The compositions of the sorbents are given in Table 1.

2. Desulfurization and Regeneration Experiments

Desulfurization experiments in a temperature range of 200-400 °C were carried out in a vertical fixed-bed tubular quartz reactor with an internal diameter of 2 cm. The bed was loaded with 1.2 g of sorbent. After the desired reaction temperature was reached, the simulated gas was fed to the fixed-bed reactor. The outlet gas concentration (H_2S and COS) was continuously measured by a gas chromatographer (GC) with a flame photometric detector (FPD) and a thermal conductivity detector (TCD). The exit H_2S (COS) concentration was monitored continuously until it almost increased to the value at the inlet. The coke oven gas composition (0.345% H_2S, 0.014% COS, 7.38% CO, 2.65% CO_2, 26.55% CH_4, and H_2) and schematic diagram of the sulfidation experimental setup can be found elsewhere [9,12]. SO_2 in the flue gas activation method was used for regeneration of sorbents. Regeneration experiments of desulfurization sorbent were carried out in a vertical fixed-bed tubular quartz reactor in a 1 vol% SO_2/Ar mixture (space velocity of 3,000 ml $h^{-1}g^{-1}$) at 700 °C until there was no elemental sulfur formation, or the concentration of SO_2 at the inlet and the outlet was equal.

Table 1. The loading level, conversion and sulfur uptake capacity of sorbent F10

Method	Content of active component (%)	m_{H_2S} (mg)	X_i (mg_{H_2S}/ $g_{active\ component}$)	Y_i (%)
MSF10	1.2	10.9	9.1	55.6
UAIF10	2.3	30.5	26.3	80.2
HPIF10	9.8	145.6	112.0	73.8

The loading capacity of the sorbents were calculated by correlating the normalized activity curves obtained with and without the sorption unit (Eq. (1)). The mass of adsorbed sulfur containing species was calculated from the difference between the H_2S and COS mass, which passed the reactor until breakthrough time, and the mass of H_2S and COS, which passed the reactor without the sorption unit until the breakthrough activity was reached (Eq. (2)). The conversion of the sorbents (Y_i) was calculated by Eq. (3).

$$X_i = \frac{m_{H_2S,\,sor}}{m_{Char}} \tag{1}$$

$$m_{H_2S,\,sor} = \frac{\nu_{sp} V_{bj} M_s}{V_m} \times \left[\int_0^t (C_{in} - C_{out})dt\right] \times 10^{-4} \tag{2}$$

$$Y_i = \frac{X_i}{\text{Theroretical loading capacities of sorbent}} \times 100\% \tag{3}$$

where, X_i is the loading capacities of sorbent; $m_{H_2S,\,sor}$ is mass of adsorbed H_2S; ν_{sp} is the space velocity (h^{-1}); V_{bj} is the volume of sorbents in the reactor (L); M_s is molar weight of sulfur (32 g/mol); m_s is the weight of sorbent in the reactor (g); V_m is molar volume of H_2S at 1atm and 25 °C (24.5 *l*/mol); t is the breakthrough time of sorbent (h); C_{in} and C_{out} are the inlet and outlet concentration of H_2S (COS) (ppmv), respectively; m_r is the mass of active components after desulfurization reaction, m_a is the amount of the total component active and Y_i is the conversion of the sorbent. Theoretical loading capacities of the sorbents were calculated from real uploading content of all active components from impregnation solution which fully reacted with hydrogen sulfide and carbonyl sulfide, and was defined as the mass of sulfur adsorbed by 100 g sorbent.

3. Sorbents Characterization

The BET surface area (Brunauer-Emmett-Teller) analysis of the sorbents was carried out with a pore size analyzer (ASAP2020) using N_2 gas adsorption method. Specific surface area and pore volume were calculated based on N_2 adsorption isotherm. The t-plot theory was employed to calculate the micro pore surface area (S_{Mi}) and micro pore volumes (V_{Mi}) [10,25].

Inductively coupled plasma-atomic emission spectrometry (ICP-AES WLY100-1, Beijing Haiguang) was used to measure the chemical composition of the sorbents. X-ray powder diffraction (Shimadzu XRD-7000, 30 mA and 40 kV) was used to identify the phases of active components in the sorbents. The XRD spectra

were obtained using Cu Kα radiation in the range of 10° to 90° at a scan rate of 5° min^{-1}.

A Thermo-Fisher Nicolet IS5 mid-FTIR spectrometer was used to examine the chemical structure of the sorbents. The specimens were prepared by mixing 1 mg of sorbent with 120 mg of KBr. Infrared spectra of the sorbent samples were obtained for the 4,000-400 cm^{-1} region.

RESULTS AND DISCUSSION

1. Effect of Different Preparation Methods on the Removal of H_2S and COS

The desulfurization performance of HPIF10 sorbent with different preparation methods at 300 °C is shown in Fig. 1. It can be seen that the preparation method of the sorbent had a significant effect on desulfurization performance of sorbent. Fig. 1(a) shows that the desulfurization efficiency of sorbent HPIF10 was maintained at 100% for 1,305 min. The breakthrough time of HPIF10 was considerably longer than that of the sorbents prepared by mechanical stirring (MS), ultrasonic assisted impregnation (UAI) methods. Breakthrough time of the MS and UAI sorbents was 156 min and 347 min, respectively. The loading capacity and mass of adsorbed H_2S of MSF10 and UAIF10 sorbents were 10.9 and 30.5, 9.1 and 26.3, respectively. However, the loading capacity and mass of adsorbed H_2S and COS of HPIF10 sorbent were 145.6 and 112, respectively. Exit COS concentrations during desulfurization followed a similar trend (Fig. 1(b)). These results indicated that char supported iron based sorbents can remove H_2S and COS simultaneously. Pore structure of acid washed coal can be effectively improved by high pressure impregnation. Liquid pressure is very high in the autoclave, giving the liquid great penetrating ability and dissolving capacity under high temperature and pressure. The hot solution can open blocked pores of the acid-washed coal, improving its pore structure. The loading capacities and conversion of sorbent F10 and the mass of adsorbed H_2S and COS are presented in Table 1. As seen in Table 1, the maximum conversion of the active components was 80.2% for the UAIF10 sorbent, which was higher than that of MS and HPI sorbents (55.6% and 73.8%, respectively). However, the active component content loaded on the HPIF10 sorbent was greater than that of the other two sorbents (MSF10 and UAIF10), which is beneficial for the removal of sulfur gases. These results are consistent with the aforementioned analysis of desulfurization of sorbent under different preparation methods.

The structure of fresh sorbents was characterized by XRD technique. The XRD spectra of different F10 sorbents with different preparation methods are shown in Fig. 2. The diffraction peaks of Fe_3O_4 and SiO_2 were observed in the XRD patterns of char supported iron sorbent with different preparation methods, which indicated that Fe_3O_4 was the active component loaded into the char for removing the H_2S and COS from the COG. The Fe_3O_4 particle size has an important effect on the removal of H_2S and COS. The smaller size of Fe_3O_4 crystals results in a higher desulfurization reactivity of sorbents. The average particle sizes of Fe_3O_4 calculated by Scherrer equation in Fe_3O_4 supported on the char by MS, UAI and HPI were 4.6 nm, 2.5 nm and 3.9 nm, respectively [4]. These results indicated that ultrasonic impregnation method can decrease the particle size and improve dispersion of active components on lignite char, but the loading of active component of sorbent was very low. The average particle size of Fe_3O_4 on HPIF10 sorbent prepared by high pressure impregnation was 3.9 nm, which is

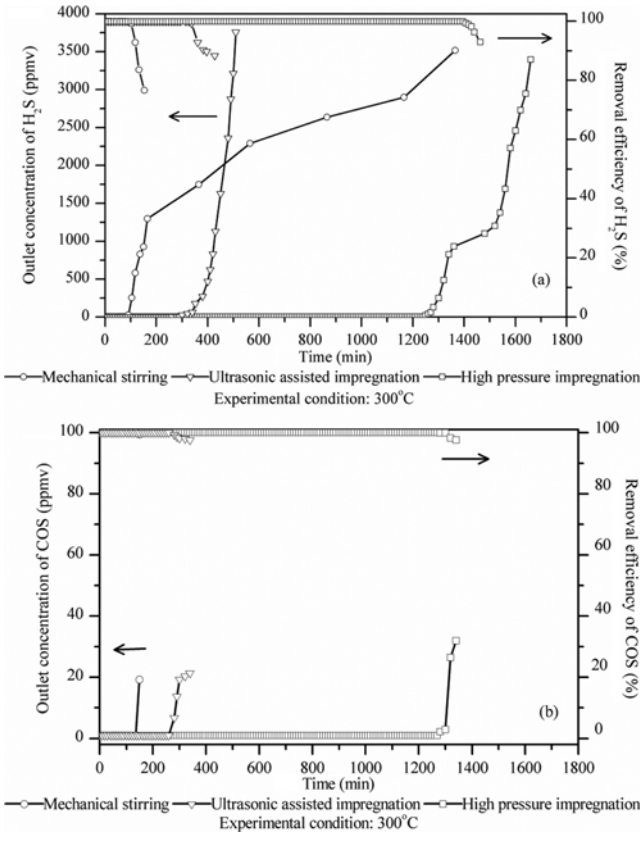

Fig. 1. Desulfurization performance of char supported iron sorbent with different preparation methods at 300 °C: (a) Desulfurization efficiency and exit concentration of H_2S vs. time; (b) desulfurization efficiency and exit concentration of COS vs. time.

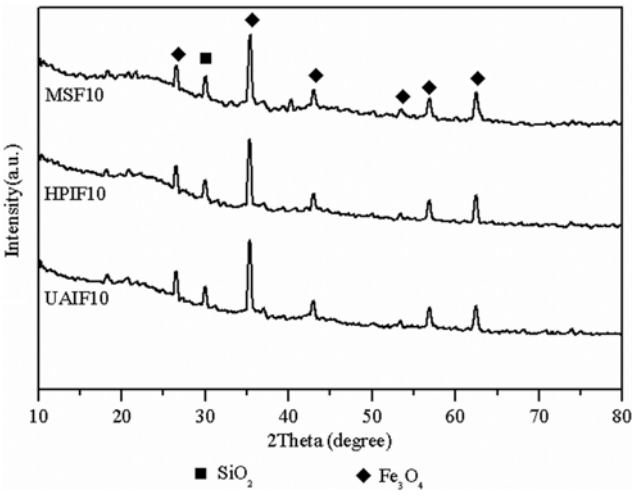

Fig. 2. XRD spectra of F10 sorbent prepared by different methods.

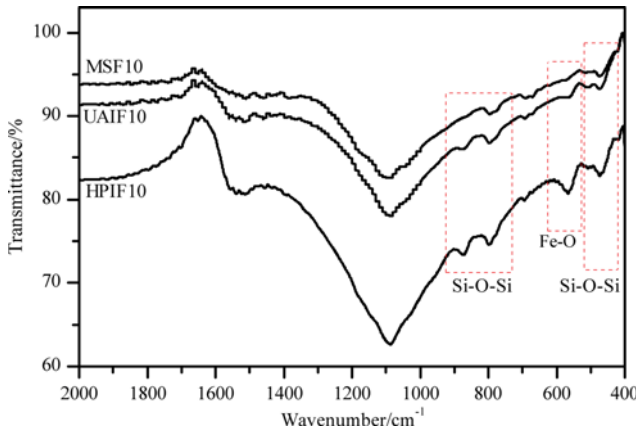

Fig. 3. FTIR spectra of F10 sorbent prepared by different methods.

beyond the pore size of char (0.80 nm). The average particle size of Fe_3O_4 on other samples prepared with MS and UAI was also beyond the pore size of char.

Fig. 3 shows the FTIR spectra of MSF10, UAIF10 and HPIF10 sorbents. Absorption bands at 1,228, 1,080, 807, and 465 cm^{-1} corresponded to the symmetrical and the asymmetrical stretching and bending vibration modes of Si-O bonds [26,27]. The spectra of Fe showed two sub-bands (at approximately 547 and 466 cm^{-1}), which correspond to the dipole movements of hematite [28]. It can be seen that the absorption bands of Fe-O for sorbent HPIF10 had higher intensity compared to MS and UAI methods. Thus, it can be also concluded that the metal oxide content of HPIF10 sorbent was higher than that of the other two sorbents (UAIF10 and MSF10). This is in agreement with ICP results.

Based on the IUPAC analysis, the sorbent showed a type-II isotherm with uniform pore size distribution [29]. The structural parameters of the sorbents are presented in Table 2. The surface area of MSF10, UAIF10 and HPIF10 sorbents was 148.02, 194.80, and 207.36 (m^2/g), respectively. The comparison showed that the HPIF10 sorbent had larger surface area and pore volume compared with the other two sorbents, which indicated that the HPI method can increase the surface area and pore structure of char. This was attributed to the high liquid pressure in the autoclave [16], which increases the penetration capability and dissolving capacity under high temperature and pressure. The average pore diameter of HPIF10 sorbent was also the largest among all sorbents. The hot solution can open blocked pores of the char, improving its pore structure. The diameter of H_2S molecule is smaller than the pores in the sorbents. This allows the H_2S molecules to easily diffuse into the inner surface of char, increasing the contact area between active component and H_2S [10].

Table 2. Physical structure parameters of different sorbents

Methods	S_{BET} (m^2/g)	S_{Mi} (m^2/g)	V_t (cm^3/g)	V_{Mic} (cm^3/g)	D_a (nm)
Char	62.59	58.38	0.18	0.03	0.80
MSF10	148.02	100.16	0.16	0.072	1.68
UAIF10	194.80	88.76	0.16	0.079	1.65
HPIF10	207.36	109.10	0.17	0.053	2.14

*S_{BET}: total surface area; S_{Mi}: microporous surface area; V_t: total pore volume; V_{Mic}: micro pore volume; D_a: average pore diameters

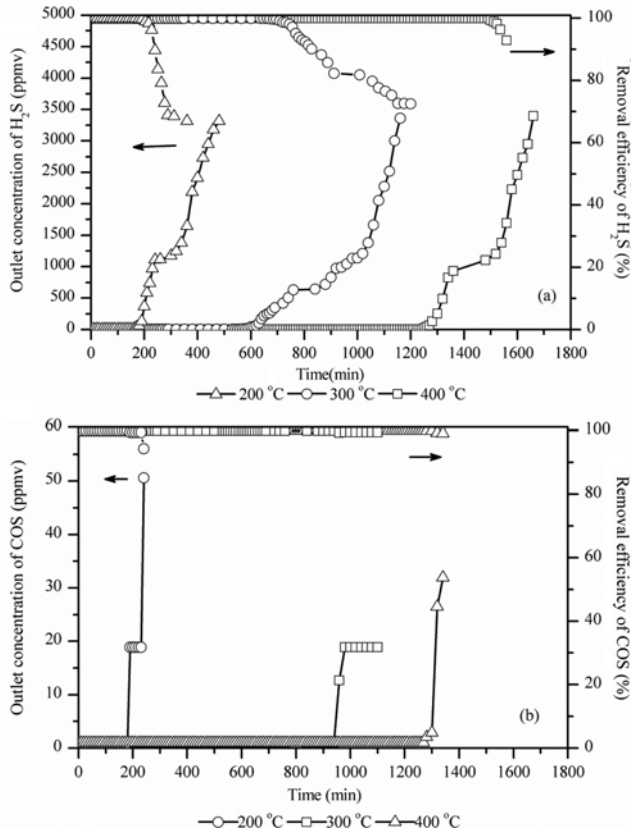

Fig. 4. Desulfurization performance of char-supported iron sorbent at different reaction temperatures: (a) Desulfurization efficiency and exit concentration of H_2S vs. time; (b) desulfurization efficiency and exit concentration of COS vs. time.

2. Effect of Desulfurization Temperature on Performance of HPIF10 Sorbent

Fig. 4 shows the desulfurization performance of HPIF10 at different temperatures. The breakthrough time and desulfurization efficiency of HPIF10 sorbent increased significantly with increasing the temperature from 200 °C to 400 °C during H_2S and COS removal. Desulfurization efficiency of sorbent at 99.5% only lasted 195 min when exit concentration of H_2S reached 50 ppmv at 200 °C. The HPIF10 sorbent was deactivated during H_2S removal after 600 min at sulfidation temperature of 300 °C. At 200 and 300 °C, the loading capacity of sorbent was 16 (mg S/g sorbent) and 53 (mg S/g sorbent), respectively. At 400 °C, the HPIF10 sorbent maintained high desulfurization efficiency (100%) for about 1,305 min and exhibited the highest loading capacity of sorbent (112 mg S/g sorbent). The breakthrough time and desulfurization efficiency for removal of COS were nearly the same as that for removal of H_2S (Fig. 4(b)), which indicated that HPIF10 sorbent could remove H_2S simultaneously with COS at all sulfidation temperatures. Because the sulfidation reaction is a non-catalytic gas-solid reaction, temperature can affect the chemical reaction and diffusion velocity of gas. Therefore, desulfurization temperature is an important factor

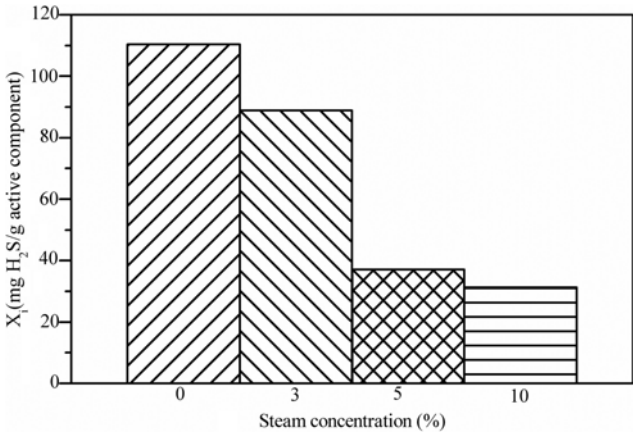

Fig. 5. Breakthrough sulfur capacity of HPIF10 sorbent as a function of steam concentration.

during removing the sulfur containing species. These results indicated that the sulfur capacity of sorbents was enhanced with increasing sulfidation temperature and reached its maximum value at 400 °C in all cases. Therefore, the reaction temperature of 400 °C was selected as the optimum desulphurization temperature.

3. Effect of Steam on the Desulfurization Performance of HPIF10 Sorbent

Steam is generally one of the components of COG, the amount of which depends upon the type of coal. Fig. 5 shows the effect of the presence of steam in COG on the desulfurization performance of char supported iron sorbent. It can be seen that the sorbent exhibited the highest loading capacity (112 mg S/g sorbent) in the absence of steam. When the steam content was 3%, loading capacity of the sorbent (88 mg S/g sorbent) was less than the highest loading capacity. However, the loading capacity of sorbent decreased remarkably with an incremental increase of steam content, especially when the steam content was more than 5%. According to the reaction equation: $Fe_3O_4+H_2S=Fe_{1-x}S+H_2O$, if the chemical reaction quotient, $[H_2O]/[H_2S]$ is thermodynamically larger than the equilibrium constant, the aforementioned sulfidation reaction occurrs inversely [30]. Therefore, when competitive reactions between Fe_3O_4/H_2S and H_2O take place, the high steam content in coke oven gas greatly suppresses the process of COG desulfurization. It can be seen that the breakthrough time of sorbent HPIF10 was the longest, and the removal efficiency was the highest when the dry COG (without steam) was used (Fig. 6). Some researchers have reported that reaction between H_2S and Fe_3O_4 is mainly surface-controlled [31,32]. When the steam content in the COG was lower than 5%, HPIF10 sorbent still showed a high sulfur capacity and removal efficiency, and the H_2S concentration in the outlet was lower than 10 ppmv. Hence, the high steam content in the COG caused a significant challenge during the desulfurization of HPIF10 sorbent.

4. Regeneration of HPIF10 Sorbent

From the economic point of view, the regeneration of sorbent is a key factor for successful char supported iron sorbent performance, since the preparation cost of lignite char support is reduced. Char supported iron sorbents are mostly regenerated by using

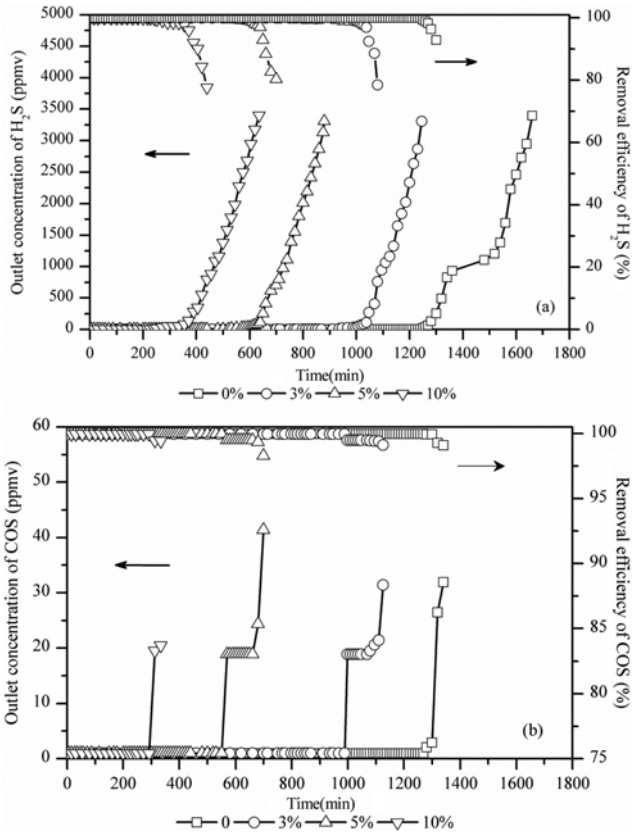

Fig. 6. Desulfurization performance of char supported iron sorbent at different steam concentrations: (a) Desulfurization efficiency and exit concentration of H_2S vs. time; (b) desulfurization efficiency and exit concentration of COS vs. time.

diluted O_2 and steam. However, O_2 and steam may cause carbon consumption of lignite chars. Alternatively, SO_2 in the flue gas can be used for regeneration of sorbent. The 1.0 vol% SO_2/N_2 mixture gas was used as the regeneration agent, and HPIF10 sorbent was regenerated for seven consecutive sulfidation/regeneration cycles at 700 °C. This temperature was used based on the authors' previous study on regeneration of char-supported sorbents [33]. According to the thermodynamic analysis (Eq. (4) and (5)), the regeneration reactions are exothermic.

$$SO_2(g)+Fe_2S_3=2FeO+4S \qquad \Delta H700\,^{\circ}C=148.1\ KJ/mol \tag{4}$$

$$2SO_2(g)+1.5Fe_2S_3=Fe_3O_4+6.5S \qquad \Delta H700\,^{\circ}C=83.9\ KJ/mol \tag{5}$$

The desulfurization-regeneration cycles of HPIF10 sorbent are shown in Fig. 7. As seen, the H_2S and COS breakthrough curves are similar in shape in each cycle, and the S adsorption content was between 112 and 86.3 mg S/g active component, which was 73.8-56.9% of theoretical S adsorption content (151.8 mg S/g active component). These results indicated that HPIF10 sorbent was stable with complete regeneration capability, showing a stable desulfurization performance after the fifth desulfurization-regeneration cycles. However, desulfurization performance of sorbent was decreased between the sixth and seventh desulfurization-regeneration cycles. After these cycles, the S adsorption content was 75.5

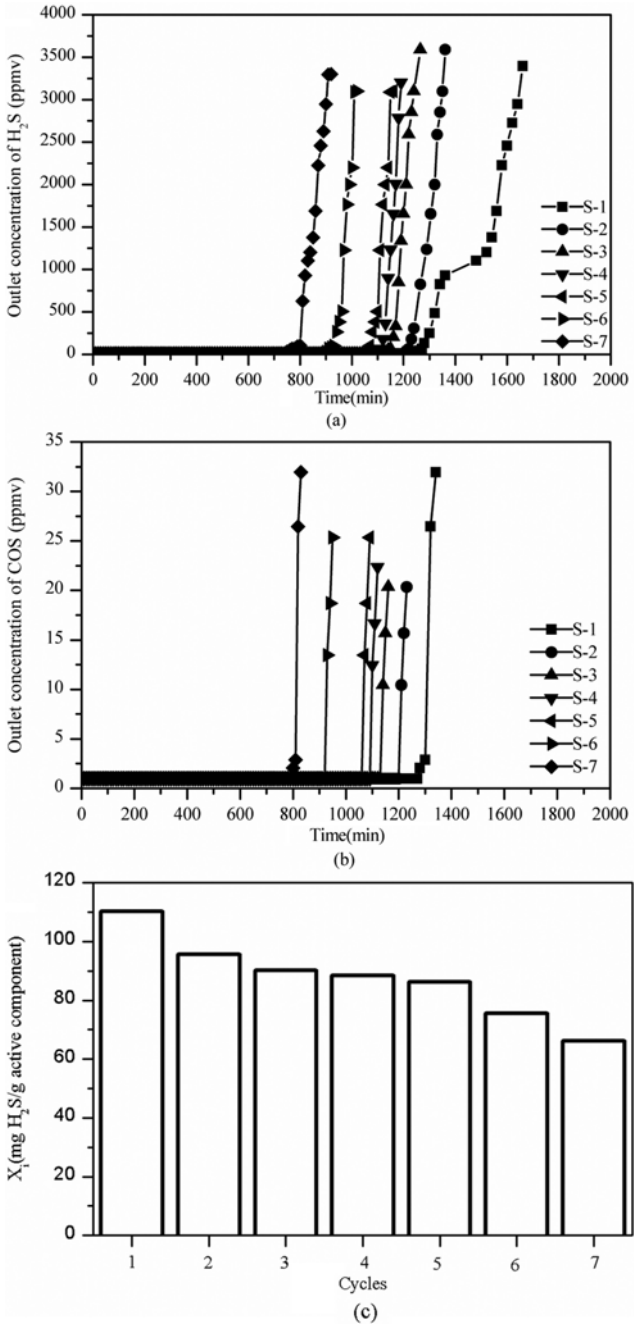

Fig. 7. H_2S and COS breakthrough curves over desulfurization-regeneration cycles of HPIF10 sorbent: (a) H_2S vs. time (b) COS vs. time (c) S adsorption content of HPIF10 sorbent over desulfurization-regeneration cycles; (Regeneration conditions: 700 °C; 1 vol% SO_2/N_2 mixture).

and 66.1 mg S/g active component, respectively, which was 49.7% and 43.5% of theoretical S adsorption content (151.8 mg S/g active component) (Fig. 7(c)). This can be attributed to the collapse of internal porous structure of sorbent, which in turn resulted in reduced exposed active sites and a poor desulfurization performance of regenerated sorbent after the sixth cycle. Metallic species impregnated on char matrix played a significant role in desulfurization and regeneration as evidenced by XRD results. XRD spectra of HPIF10 sorbent after regeneration by SO_2 are shown in Fig. 8. As can be seen, metal sulfide (iron sulfide) was transformed into corresponding metal oxides (Fe_3O_4) as predominant phase after SO_2 regenerated. The average particle sizes of Fe_3O_4 after regeneration (from R1 to R7) calculated by Scherrer equation in Fe_3O_4 supported on the char was 4.6 nm, 5.3 nm, 5.6 nm, 6.0 nm, 6.5 nm, 6.6 nm, and 6.9 nm, respectively. After several desulfurization-regeneration cycles, the physical structure of sorbent was destroyed and the active components were unevenly dispersed on the surface of char and formed larger particles during regeneration reactions. Metal sulfide ($Fe_{1-x}S$) was also detected in the sorbent after fifth desulfurization-regeneration cycles. These results further confirmed that the superior sulfidation properties of HPIF10 sorbent can be maintained for five desulfurization-regeneration cycles.

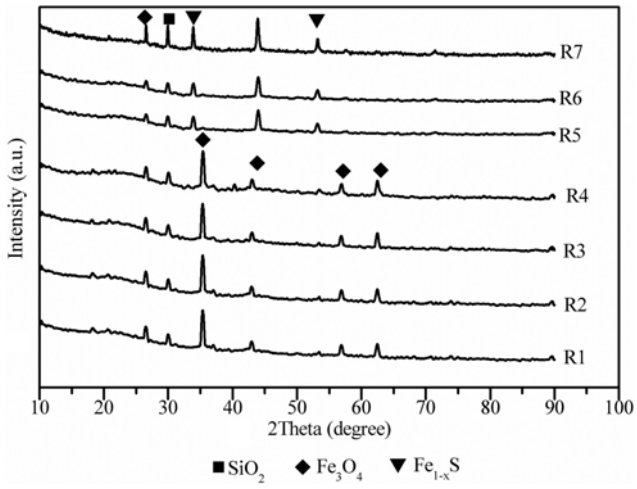

Fig. 8. XRD spectra of HPIF10 sorbent after several sulfidation-regeneration cycles.

Table 3. Physical structure parameters of char supported iron sorbent after multiple tests

Cycles	S_{BET} (m^2/g)	S_{Mi} (m^2/g)	V_t (cm^3/g)	V_{Mic} (cm^3/g)	D_a (nm)
R1	203.50	103.23	0.18	0.065	2.35
R2	195.36	101.65	0.17	0.062	1.98
R3	186.49	97.34	0.17	0.060	1.80
R4	177.32	92.21	0.15	0.056	1.76
R5	160.37	82.16	0.10	0.055	1.51
R6	152.62	79.36	0.12	0.053	1.50
R7	141.78	63.27	0.10	0.050	1.46

*S_{BET}: total surface area; S_{Mi}: microporous surface area; V_t: total pore volume; V_{Mic}: micro pore volume; D_a: average pore diameters

Physical structure parameters of char supported iron sorbent after multiple tests are given in Table 3. As seen, with increasing the number of desulfurization-regeneration cycles, the surface area and average pore diameter of sorbents were decreased, which indicated that the char structure was destroyed and some pores were blocked as a consequence of multiple sulfidation and regeneration. These changes in the textural properties of sorbents after multiple

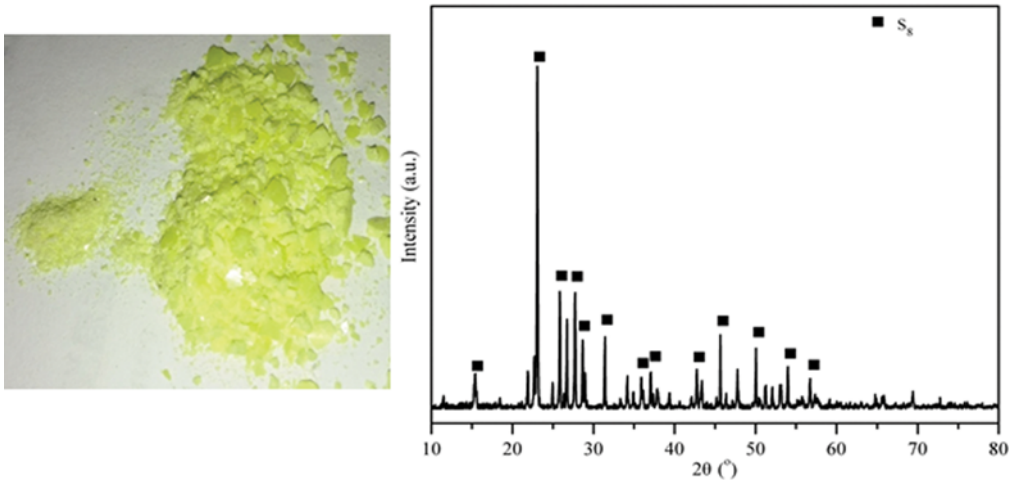

Fig. 9. XRD spectra of elemental sulfur formed during regeneration.

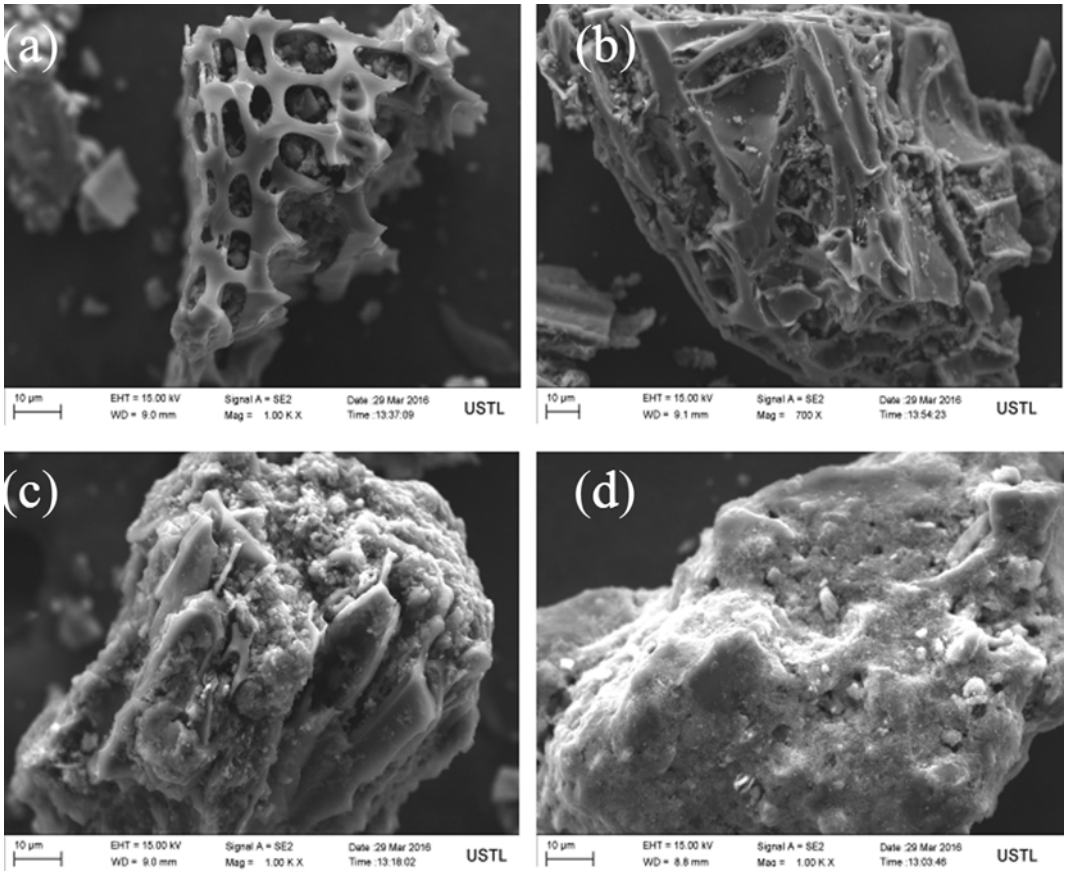

Fig. 10. SEM-EDS analysis of different samples: (a) Fresh desulfurization sorbent, (b) HPIF10 sorbent after regeneration in the 1st cycle, (c) HPIF10 sorbent after regeneration in the 3rd cycle, (d) HPIF10 sorbent after regeneration in the 5th cycle.

desulfurization-regeneration cycles resulted in decreased desulfurization efficiency.

Elemental sulfur was formed during regeneration using 1% SO_2/N_2 mixture (Fig. 9). It has been reported that monoclinic sulfur can be produced when the reaction temperature is higher than 95.6 °C, and it can be melted when temperature exceeds 119 °C [34]. However, the monoclinic sulfur can be changed to rhombic sulfur at lower temperature when the reaction is completed. As a high regeneration temperature (700 °C) was used in this study, the elemental sulfur was vaporized and released from the pore surface of sorbent.

Figs. 10(a)-10(d) show the SEM images of the fresh desulfurization sorbent, and sorbents after first, third, and fifth cycles, respectively. Fig. 10(a) shows some clusters with a good macroporosity composed of many non-spherical particles in fresh desulfuriza-

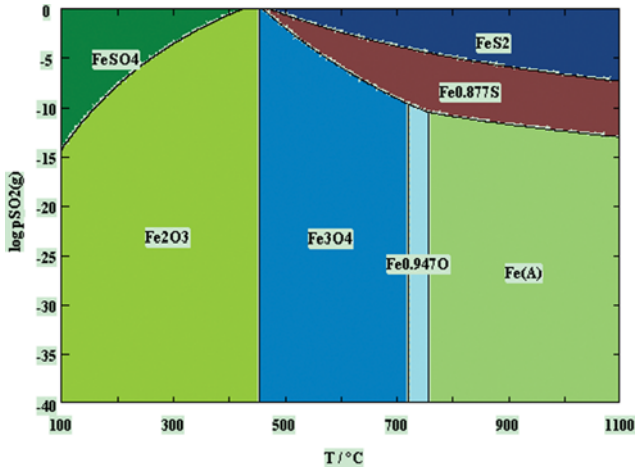

Fig. 11. Thermodynamic analysis of iron-based sorbents as a function of SO_2 partial pressure and temperature.

tion sorbent. After the first cycle (Fig. 10(b)), a slight growth in the average size of the clusters was observed. After the third cycle, the structure of the HPIF10 was still maintained and the surface of the particles was covered with some fine fragments. However, after fifth cycle, the structure of HPIF10 was destroyed and some pores were blocked as a consequence of multiple sulfidation and regeneration cycles. The SEM images implied that the porosity of desulfurization sorbent samples decreased to some extent and a distinct tendency of a mild agglomeration was also seen during the five desulfurization-regeneration cycles.

Thermodynamic phase diagrams for the sorbent at different temperatures are shown in Fig. 11. It can be seen that Fe_2O_3 and Fe_3O_4 are preferred over Fe as the thermodynamically stable phase at lower temperatures. Higher concentration of SO_2 and lower temperatures also favored $Fe_{1-x}S$ reaction with SO_2 to form Fe_2O_3 and Fe_3O_4. Regeneration of sorbent using SO_2 can form Fe_3O_4 and elemental sulfur in the temperature range of 500-700 °C. The regeneration of sorbent at medium temperatures with higher partial pressure of SO_2 is favorable. This agrees well with our previous study [33].

CONCLUSIONS

The HPI method significantly enhanced the desulfurization performance of char-supported iron sorbents during the COG desulfurization, in particular the desulfurization efficiency. The high pressure impregnation method increased the surface area and pore structure of sorbent.

The presence of steam in the coke oven gas inhibited the desulfurization performance of sorbent. SO_2 regeneration of used sorbents resulted in formation of elemental sulfur. The HPIF10 sorbent showed good stability during five desulfurization-regeneration cycles without changing its performance significantly.

ACKNOWLEDGEMENTS

We gratefully acknowledge the financial support of Nation Natural Science Foundation of China (21176109, U1361120, 21476100).

REFERENCES

1. K. Y. Koo, J. H. Lee, U. H. Jung, S. H. Kim and W. L. Yoon, *Fuel*, **153**, 303 (2015).
2. R. Razzaq, C. Li and S. Zhang, *Fuel*, **113**, 287 (2013).
3. J. M. Bermúdez, N. Ferrera-Lorenzo, S. Luque, A. Arenillas and J. A. Menéndez, *Fuel Process. Technol.*, **115**, 215 (2013).
4. Z. F. Qin, J. Ren, M. Q. Miao, Z. Li, J. Y. Lin and K. C. Xie, *Appl. Catal. B-Environ.*, **164**, 18 (2015).
5. Y. C. Park, S. H. Jo, H. J. Ryu, J. H. Moon, C. K. Yi, Y. Yoon and J. I. Baek, *Korean J. Chem. Eng.*, **29**, 1812 (2012).
6. J. He, J. Shang, Q. Li, W. Xu, J. Liu, X. Feng and T. Zhu, *J. Hazard. Mater.*, **271**, 89 (2014).
7. B. L. Dou, C. Wang, H. S. Chen, Y. C. Song, B. Z. Xie, Y. J. Xu and C. Q. Tan, A review, *Chem. Eng. Res. Des.*, **90**, 1901 (2012).
8. N. Fukuda, M. Takaoka, S. Doumoto, K. Oshita, S. Morisawa and T. Mizuno, *Atmos. Environ.*, **45**, 3685 (2011).
9. J. Dou, J. Yu, A. Tahmasebi, F. Yin, S. Gupta, X. Li, J. Lucas, C. Na and T. Wall, *Fuel Process. Technol.*, **135**, 187 (2015).
10. J. Dou, X. Li, A. Tahmasebi, J. Xu and J. Yu, *Korean J. Chem. Eng.*, **32**, 2227 (2015).
11. F. Yin, J. Yu, J. Dou, S. Gupta, B. Moghtaderi and J. Lucas, *Energy Fuels*, **28**, 2481 (2014).
12. J. Yu, F. Yin, S. Wang, L. Chang and S. Gupta, *Fuel*, **108**, 91 (2013).
13. X. Zhang, X. Zheng, P. Han, Z. Liu and L. Chang, *J. Energy Chem.*, **24**, 291 (2015).
14. J. Mi, J. Ren and Y. Zhang, *Environ. Eng. Sci.*, **29**, 1026 (2012).
15. X. Ren, Q. He, Y. Dong, M. Wang, L. Chang and W. Bao, *Energy Fuels*, **28**, 4746 (2014).
16. X. R. Zheng, W. R. Bao, Q. M. Jin, L. P. Chang and K. C. Xie, *Energy Fuels*, **25**, 2997 (2011).
17. F. Yin, J. Yu, S. Gupta, S. Wang, D. Wang and J. Dou, *Fuel Process. Technol.*, **117**, 17 (2014).
18. B. Zeng, H. R. Yue, C. J. Liu, T. Huang, J. Li, B. Zhao, M. Zhang and B. Liang, *Energy Fuels*, **29**, 1860 (2015).
19. D. Liu, S. Y. Chen, X. Y. Fei, C. J. Huang and Y. C. Zhang, *Ind. Eng. Chem. Res.*, **54**, 3556 (2015).
20. B. Guo, L. P. Chang and K. C. Xie, *Ind. Eng. Chem. Res.*, **53**, 8874 (2014).
21. J. J. Park, C. G. Park, S. Y. Jung, S. C. Lee, D. Ragupathy and J. C. Kim, *Res. Chem. Intermed.*, **37**, 1193 (2011).
22. J. Dou, A. Tahmasebi, F. Yin and J. Yu, *Environ. Progress*, **35**, 352 (2016).
23. M. Chomiak and J. Trawczynski, *Fuel Process. Technol.*, **134**, 92 (2015).
24. Y. Zeng, S. Zhang, F. R. Groves and D. P. Harrison, *Chem. Eng. Sci.*, **54**, 3007 (1999).
25. B. S. Liu, Y. Zhang, J. F. Liu, M. Tian, F. M. Zhang and C. T. Au, *J. Phy. Chem.: C*, **115**, 16954 (2011).
26. X. Zheng, W. Bao, L. Chang, Q. Jin, R. He and K. Xie, *Energy Fuels*, **26**, 3393 (2012).
27. F. Jones, J. Farrow and W. V. Bronswijk, *Langmuir*, **14**, 6512 (1998).
28. B. E. Yoldas, *J. Non-Cryst. Solids*, **63**, 145 (1984).
29. J. Lian, X. Duan, J. Ma, P. Peng, T. Kim and W. Zheng, *ACS Nano*,

3, 3749 (2009).
30. Z. F. Zhang, B. S. Liu, F. Wang and S. Zheng, *Chem. Eng. J.*, **272**, 69 (2015).
31. S. Cheah, Y. O. Parent, W. S. Jablonski, T. Vinzant and J. L. Olstad, *Fuel*, **97**, 612 (2012).
32. Z. F. Zhang, B. S. Liu, F. Wang, C. Xia, S. Zheng and R. Amin, *Appl. Surf. Sci.*, **313**, 961 (2014).
33. Y. Feng, J. Dou, A. Tahmasebi, J. Xu, X. Li, J. Yu and F. Yin, *Energy Fuels*, **29**, 7124 (2015).
34. J. Chang, H. J. Tian, J. G. Jiang, C. Zhang and Q. J. Guo, *Chem. Eng. J.*, **291**, 225 (2016).